molecules

MDPI

Article

QM/MM Modeling of the Flavin Functionalization in the RutA Monooxygenase

Bella Grigorenko [1,2], Tatiana Domratcheva [1] and Alexander Nemukhin [1,2,*]

[1] Department of Chemistry, M.V. Lomonosov Moscow State University, Moscow 119991, Russia
[2] N.M. Emanuel Institute of Biochemical Physics, Russian Academy of Sciences, Moscow 119334, Russia
* Correspondence: anem@lcc.chem.msu.ru

Abstract: Oxygenase activity of the flavin-dependent enzyme RutA is commonly associated with the formation of flavin-oxygen adducts in the enzyme active site. We report the results of quantum mechanics/molecular mechanics (QM/MM) modeling of possible reaction pathways initiated by various triplet state complexes of the molecular oxygen with the reduced flavin mononucleotide (FMN) formed in the protein cavities. According to the calculation results, these triplet-state flavin-oxygen complexes can be located at both *re*-side and *si*-side of the isoalloxazine ring of flavin. In both cases, the dioxygen moiety is activated by electron transfer from FMN, stimulating the attack of the arising reactive oxygen species at the C4a, N5, C6, and C8 positions in the isoalloxazine ring after the switch to the singlet state potential energy surface. The reaction pathways lead to the C(4a)-peroxide, N(5)-oxide, or C(6)-hydroperoxide covalent adducts or directly to the oxidized flavin, depending on the initial position of the oxygen molecule in the protein cavities.

Keywords: flavin; monooxygenases; RutA enzyme; molecular oxygen; quantum chemistry; QM/MM; absorption spectra

Citation: Grigorenko, B.; Domratcheva, T.; Nemukhin, A. QM/MM Modeling of the Flavin Functionalization in the RutA Monooxygenase. *Molecules* **2023**, *28*, 2405. https://doi.org/10.3390/molecules28052405

Academic Editor: Cecilia Coletti

Received: 27 January 2023
Revised: 21 February 2023
Accepted: 3 March 2023
Published: 6 March 2023

1. Introduction

Flavoprotein monooxygenases are involved in multiple metabolic processes [1]. The monooxygenase RutA is one of seven proteins on the Rut pathway, which are required by *Escherichia coli* (strain K12) to grow on uracil as the sole nitrogen source [2]. The flavoenzyme RutA directly cleaves the uracil ring between N3 and C4 to yield ureidoacrylate, as established by nuclear magnetic resonance spectroscopy and mass spectroscopy. However, a mechanism for this reaction is still a matter of discussion; in particular, it is required to explain how RutA incorporates an oxygen atom from O_2 at the proper position of uracil. Flavoenzymes are able to control chemical reactions involving the oxygen molecule in the absence of metal or metal-containing cofactors. These enzymes exploit the properties of the flavin's isoalloxazine ring to activate dioxygen and initiate productive reactions, often with the assistance of transient covalent flavin-oxygen adducts [3]. Recent results of experimental studies of RutA stimulated discussion of the factors that govern oxygenase activity in flavoenzymes, including the role of various flavin-oxygen adducts [4–7].

The active site in RutA stabilizes the reduced form of flavin mononucleotide (FMN), which is non-covalently bound in the solvent-accessible protein cavity. Scheme 1 shows the reduced (Fl_{red}) and oxidized (Fl_{ox}) forms of FMN and the common numbering of atoms in the isoalloxazine ring. According to current knowledge [3,5–7], when the oxygen molecule is trapped in a protein cavity near the isoalloxazine ring, it is activated by an electron transfer from the reduced FMN. This leads to a pair of the superoxide radical (O_2^-) and the relatively stable semiquinone radical (Fl_{SQ}), followed by the switch from the initial triplet spin state to the singlet spin state. The reactive C4a-N5 locus of the isoalloxazine moiety is usually considered a critical site for dioxygen (O_2) activation and subsequent covalent adduct formation. These adducts, flavin-C(4a)-peroxide and flavin-N(5)-oxide,

are recognized as the key oxygen-transferring intermediates in the catalytic mechanisms of the flavoprotein monooxygenases and oxidases [3].

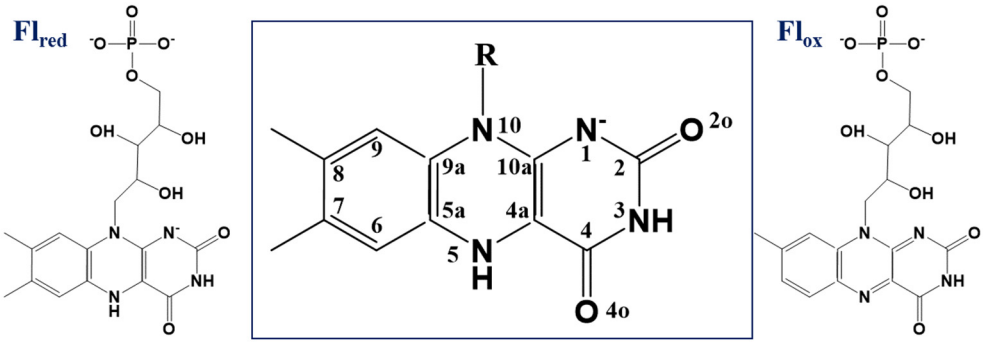

Scheme 1. Reduced FMN (left), oxidized FMN (right), and atom numbering in the isoalloxazine ring of flavin (center).

According to the findings described in [6], the primary catalytic mechanism in RutA (as well as in the other flavoenzyme, EncM [8]) is associated with N5-oxigenation. Matthews et al. [6] conducted O_2-pressurized X-ray crystallography at 5 or 15 bars and produced crystals of RutA that contained oxidized FMN and molecular oxygen (RutA–Fl$_{ox}$–O_2). The crystal structure PDB ID 6SGG was interpreted as the model containing the dioxygen moiety next to the N5 atom of the isoalloxazine ring with an unusually short distance of 2.09 Å between one of the oxygen atoms in O_2 and the N5 atom of the flavin [6]. An important role of the amino acid residues Thr105 and Asn134 in forming the protein cavity at the *re*-side of the flavin cofactor was underlined upon dioxygen binding [6]. The crystal structure for the complex RutA–Fl$_{ox}$–uracil was also produced (PDB ID 6SGL) [6]. The stopped-flow kinetics studies revealed that in the absence of uracil, the reduced form of FMN bound to RutA is converted to the oxidized form—the time-resolved absorption bands showed the gradual rise of the band with the maximum at 446 nm, typical for the protein-bound Fl$_{ox}$ [8,9]. When uracil was added to the RutA–Fl$_{red}$–O_2 system, the spectra showed the mixed formation of Fl$_{ox}$ and the flavin-N(5)-oxide adduct (Fl$_{N5O}$); in particular, the band maximum was red-shifted to 463 nm, the value assigned to the Fl$_{N5O}$ species [8].

The experimental work on RutA [6] and the related flavoprotein EncM [5] also included computational modeling of the reaction pathways associated with the formation of the covalent flavin-oxygen adducts. Ref. [5] contains the results of the density functional theory (DFT) calculations at the B3LYP-D3 level for the lumiflavin (reduced)—oxygen model system in the gas-phase. The computed profiles, leading to the Fl$_{C4aOO^-}$, Fl$_{N5OOH}$, and Fl$_{N5O}$ species, were corrected within the polarizable continuum model, taking into account the water solvent effects as well as the enthalpy and Gibbs energy corrections. The basic conclusion formulated by the results of the DFT modeling is that the formation of both flavin-C(4a)-peroxide (Fl$_{C4aOO^-}$) and flavin-N(5)-oxide (Fl$_{N5O}$) is feasible. A year later, Luo and Liu [10] computed the energy profiles starting from the reduced lumiflavin and O_2 and leading to the Fl$_{C4aOOH}$ species in the gas phase (corrected within the continuum solvent models) using the DFT and complete active space self-consistent field (CASSCF) quantum chemistry methods.

To the best of our knowledge, no computational modeling of the formation of the products of the flavin-oxygen interaction inside the protein cavities in monooxygenases by the QM/MM method has been reported. Application of QM/MM calculations as compared with gas-phase-based simulations is important because the protein matrix provides a suitable cage to stimulate the triplet-singlet switch and recombination of the superoxide-Fl$_{SQ}$ radical pair to a flavin-oxygen adduct before the radical intermediates diffuse apart [7]. Thus, the enzyme-mediated stabilization of the radical intermediates should be simulated in the protein environment.

In this work, we construct the model system RutA–FMN_{red}–O_2 using the coordinates of heavy atoms in the crystal structure PDB ID 6SGG [6]. The QM(DFT)/MM method is applied to locate several structures of complexes of the triplet state oxygen molecule with the molecular groups near the flavin's isoalloxazine ring in the solvent-accessible protein cavities, i.e., the putative oxygen binding sites. The occurrence of different dioxygen positions in RutA was documented in our preliminary studies [11,12] based on molecular dynamics (MD) simulations. Here, we model the formation of products of the flavin-oxygen interaction initiated from various oxygen-binding sites.

Besides structures of the flavin-oxygen complexes in RutA, we also report here the computed excitation energies of the $S_0 \rightarrow S_1$ and $S_0 \rightarrow S_2$ transitions and the corresponding oscillator strengths (o.s.) of transient species, which provide estimates of the absorption band maxima in the electronic spectra. It is difficult to refer to large numbers of papers devoted to modeling the electronic spectra of flavin-based systems using a variety of quantum chemistry methods. We only note a recent review by Kar et al. [9], as well as the most relevant recent papers [13–15]. In this work, we apply the advanced excited-state method, the extended multi-configurational quasi-degenerate perturbation theory in the second order (XMCQDPT2) [16], which has proven its efficiency in predicting the excitation energies of organic chromophores [17–20].

2. Results and Discussion

In Figure 1, we show a general view of the model system is considered in this work. In the inset, we clarify the position of the isoalloxazine ring of FMN in the active site of the enzyme and the nearest molecular groups—the Asn134 and Thr105 side chains at the flavin's *re*-side or water molecules at the *si*-side. We found several triplet state minimum energy structures of the complex of RutA with the oxygen molecule positioned near the isoalloxazine ring using the QM/MM method (see details in Section 3 below). Atomic coordinates of all located structures are available from the supplementary materials for the present paper.

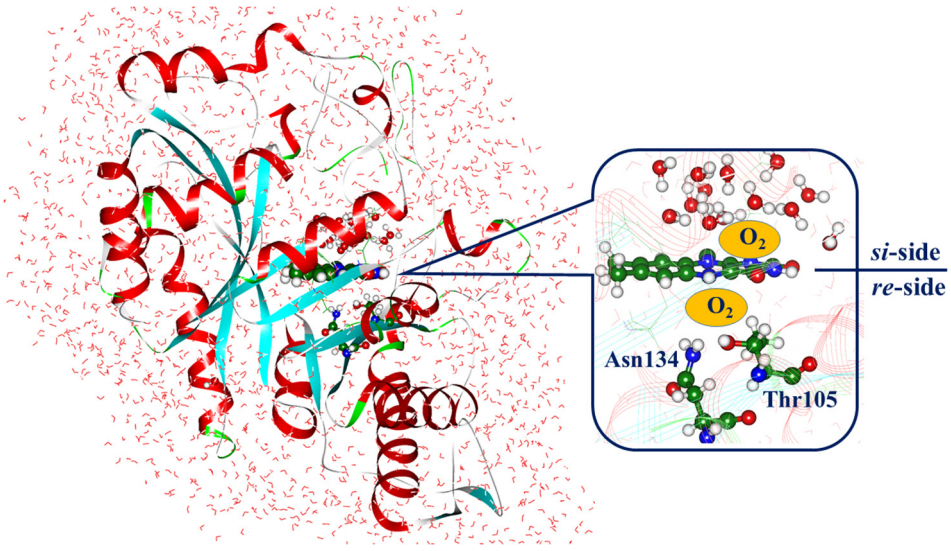

Figure 1. A general view of the model system considered in this work. Inset—the isoalloxazine ring of FMN and the nearest molecular groups at the *re*-side (Asn134 and Thr105) and at the *si*-side (water molecules). In this and other figures, carbon atoms are shown in green, oxygen in red, nitrogen in blue, and hydrogen in white.

There are several important observations related to the computationally derived model systems containing the flavin-oxygen complexes. First, the optimized positions of dioxygen are located on both sides (*re*-side and *si*-side) of the isoalloxazine ring (see Figure 1). The sites at the *re*-side correspond to the oxygen pocket-1 noted in [12], as well as the position of

oxygen in the X-ray structure PDB ID 6SGG [6]. The sites on the *si*-side, which correspond to the oxygen pocket-5 noted in [12], describe the oxygen molecule inside the shell of water molecules. Second, in each located oxygen-flavin complex, the dioxygen moiety should be identified as a superoxide O_2^- anion rather than a neutral triplet oxygen molecule. Third, the energies of the triplet and singlet states in these flavin-oxygen complexes are almost degenerate. To support the second and third conclusions, we analyze the results of the complete active space self-consistent field (CASSCF) calculations of the complexes (for details, see Section 3 below). Thus, assuming a switch from the triplet state potential energy surface (PES) to the singlet state PES, modeling a triplet-singlet intersystem crossing, several pathways to the reaction products arise, including the formation of the flavin-oxygen adducts. We describe these pathways in the following subsections using the QM(DFT)/MM calculations and characterize the excitation energies of the products using the XMCQDPT2 calculations.

2.1. Pathway-1: Formation of the C(4a)-peroxyflavin Species from the Si-Side Oxygen Pocket

As described in the Introduction, the formation of the transient C(4a)-(hydro)peroxyflavin intermediates, Fl_{C4aOOH} or $Fl_{C4aOO}{}^-$, is commonly accepted in the chemistry of flavoenzymes [3,7], even though the C(4a)-peroxyflavin species in water is unstable and dissociates to hydrogen peroxide (H_2O_2) and the oxidized flavin [3]. Previous simulations [5,10] described the reaction pathways from reduced lumiflavin (Fl_{red}) and O_2 to $Fl_{C4aOO}{}^-$ and Fl_{C4aOOH} using the continuum solvent models. In both calculations, the transition from the initial triplet state model system to the singlet state system occurs after electron transfer in the configuration of the radical pair superoxide—Fl_{SQ}. In both cases, low activation barriers of several kcal/mol were estimated.

According to the results of molecular dynamics simulations with the QM(DFT)/MM potentials for the RutA-O_2-uracil model system [12], the C(4a)-peroxyflavin species was spontaneously formed after switching from the triplet state to the singlet state system at the trajectory frames that showed the occurrence of both dioxygen and uracil near the isoalloxazine ring at the *si*-side. Complexes of RutA with dioxygen located at the *si*-side pocket are located in this work using the QM/MM method (see Section 3 below for technical details). Figure 2a shows the triplet state minimum energy structure of the complex, which is denoted here as Complex-1. In this and other figures, we show critical distances (in Å) between heavy atoms and pay attention to the hydrogen-bond patterns. The water molecules, which are the components of hydrogen-bond networks, are numbered sequentially as they appear in the figures.

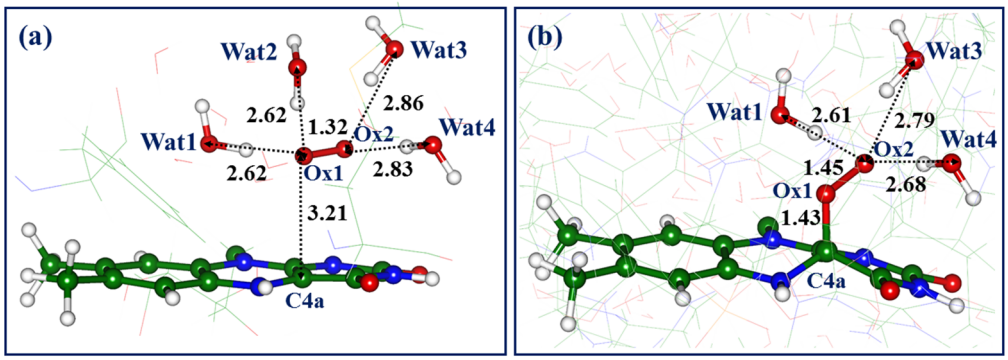

Figure 2. Pathway-1: (**a**) Triplet state complex Fl_{red}-O_2 (Complex-1) formed at the *si*-side. (**b**) Singlet state $Fl_{C4aOO}{}^-$ species. In this and other figures, distances are given in Å.

For Complex-1, we note that the Ox1-Ox2 distance in dioxygen increases from the value of about 1.20 Å in the gas-phase triplet state O_2 molecule to 1.32 Å, thus favoring the formation of the superoxide anion. The latter is hydrogen bonded to the four nearest water molecules, with typical intermolecular distances between the oxygen atoms

(2.6–2.9 Å). The C4a atom is the closest atom of the isoalloxazine ring to the dioxygen atoms, with a C4a-Ox1 distance 3.21 Å; the N5-Ox1 distance is 3.89 Å.

To characterize the electronic structure in Complex-1 in the triplet and singlet states, we carried out CASSCF(14/10)/cc-pVDZ calculations with the distribution of 14 electrons over 10 molecular orbitals. The latter include the orbitals located at the isoalloxazine ring and dioxygen (Figure 3). Orbitals 5–7 in both triplet and singlet states include notable contributions from dioxygen. Two dominant electronic configurations in the triplet Ψ_T and singlet Ψ_S wavefunctions are shown on the right side of Figure 3, indicating that the weight of the superoxide structure is considerable in the triplet state and dominant in the singlet state. Therefore, we conclude that Complex-1 bears the features of the Fl_{SQ}–O_2^- radical pair. Notably, the CASSCF energies of the triplet and singlet states (see the right side of Figure 3) are practically degenerate at this geometry since the energy gap is less than 0.1 kcal/mol. Therefore, we may assume that the switch from the triplet state PES to the singlet state PES in this model system occurs in the immediate vicinity of the geometry configuration of Complex-1.

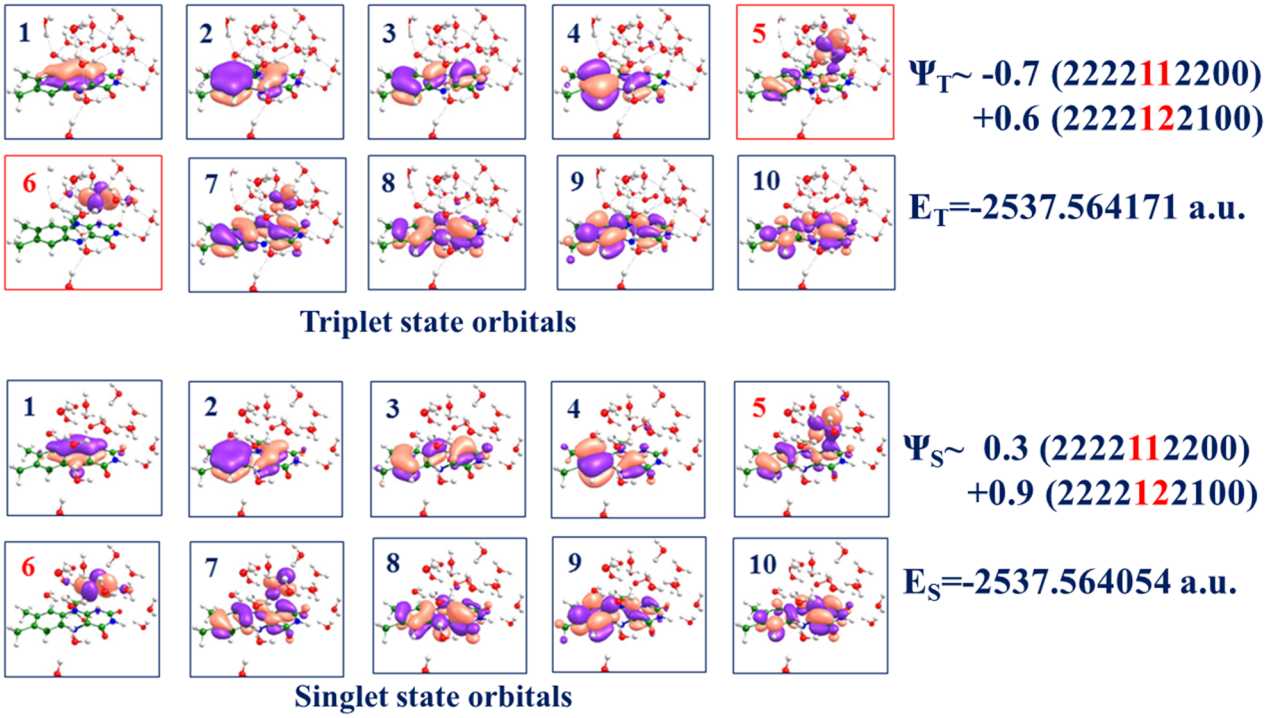

Figure 3. Results of the CASSCF(14/10)/cc-pVDZ calculations for Complex-1 (Figure 2a). The legends on the right side show dominant electronic configurations and their weights in the triplet state and singlet state CASSCF wavefunctions composed of the active orbitals illustrated in ten boxes. The occupancies of the fifth and sixth orbitals, mainly assigned to dioxygen, are distinguished by the red color.

Taking the structure of Complex-1 as a starting point for geometry optimization at the QM/MM level on the singlet state potential energy surface, we arrive at the structure shown in Figure 2b. In this system, the oxygen atom, Ox1, is covalently bound to C4a, leading to the distorted isoalloxazine ring. Another oxygen atom, Ox2, is hydrogen bonded to three water molecules; one water molecule from the initial structure, Wat2 in Figure 2a, drifted away from the dioxygen moiety. In agreement with the previous QM/MM studies of the reactions of the superoxide with the conjugated organic molecules inside proteins, e.g., with the chromophore of the green fluorescent protein [21,22], no potential energy barrier is detected on the pathway leading to the C(4a)-peroxyflavin species. The energy of the RutA structure with the C(4a)-peroxyflavin (Figure 2b) is 16.8 kcal/mol lower than the level of the reactants shown in Figure 2a.

It is instructive to compare these findings with the previously reported quantum chemistry computational results [5,10]. For the reaction of the reduced lumiflavin with the oxygen molecule, which starts at the triplet state PES and switches to the singlet state PES after an intersystem crossing (ISC) point, [10] reports the structure of the ISC point optimized at the CASSCF(12/9) level. The Ox1-Ox2 distance varies from the initial value of 1.20 Å for the reactants to the value of 1.31 Å near the ISC point to be compared to our 1.32 Å in Complex-1. The charge of the dioxygen moiety at this point is almost -1, as in the present work. The Ox1-Ox2 distance in the singlet state C(4a)-peroxyflavin adduct is 1.46 Å (versus 1.45 Å in the present work). The C4a-Ox1 distance varies from 3.14 Å (versus 3.21 Å in the present work) for the triplet state reactants to 1.41 Å (versus 1.36 Å in the present work) for the singlet state C(4a)-peroxyflavin adduct. The reaction energy profile shows the barrier of about 10 kcal/mol on the way from the initial triplet state structure of Fl^- ... O_2 to the ISC point (the corresponding reaction segment is unavailable in our simulations). The reported potential energy difference between the ISC point and the singlet state C(4a)-peroxyflavin adduct (see Table S4 in [10]) for a water solution is 14.1 kcal/mol, to be compared with the value of 16.8 kcal/mol computed for the protein environment in the present work. We conclude that Complex-1 resembles the ISC point identified in [10]. In [5], the authors report in their supplementary materials the computed potential energy difference of 8.1 kcal/mol between the C(4a)-peroxyflavin adduct and the reactants (Fl^- ... O_2) for the water solution, using the B3LYP-D/6-311++G(2d,2p) calculations. The computed energy profile shows the energy barriers on both reaction steps: from (Fl^- ... O_2) to Fl_{SQ} ... $O_2{}^-$ and then to the $Fl_{C4aOO}{}^-$ adduct.

With respect to the $S_0 \rightarrow S_1$ excitation, our XMCQDPT2 calculations (see details in Section 3 below) report the excitation energy of the model system (Figure 2b) at 3.47 eV (357 nm, 0.57 o.s.), in excellent agreement with the experimental absorption band known for the C(4a)-peroxyflavin intermediate [3].

To conclude this subsection, we emphasize that the formation of the C(4a)-peroxyflavin intermediate is a commonly accepted route in monooxygenase activity, as reproduced in our calculations. We report an interesting finding that the oxygen molecule approaches the C4a position from the *si*-side pocket, i.e., from the site, presumably occupied by a uracil substrate in RutA [6]. Simulations described in [12] show that location of both the substrate and dioxygen at the same site of the isoalloxazine ring does not prevent the formation of $Fl_{C4aOO}{}^-$; this intermediate may occur and attack the substrate. Few theoretical papers report calculations of the functionalized flavins at the position C4a, e.g., refs. [23,24].

2.2. Pathway-2: Oxygen-N5 Interaction from the Si-Side Oxygen Pocket

Another triplet-state complex of the reduced flavin with dioxygen located at the *si*-side pocket is shown in Figure 4a. The QM/MM energy of this Complex-2 is 1.5 kcal/mol lower than the energy of Complex-1, indicating that these structures may be almost equally populated. Complex-2 shares the same features with Complex-1 in the sense that the superoxide describes the dioxygen moiety in this environment—the Ox1-Ox2 distance is 1.30 Å, and the charge on dioxygen is almost -1. However, in Complex-2, dioxygen stays closer to the isoalloxazine ring—the Ox2-N5 distance (2.58 Å) is about 0.6 Å shorter than the Ox1-C4a distance of 3.21 Å in Complex-1. Complex-2 also shows different hydrogen-bonding patterns as compared to Complex-1 (cf. Figures 2a and 4a)—only two water molecules, Wat4 and Wat5 in Figure 4a, are within the hydrogen-bond distances from the dioxygen atoms; the water molecule Wat6 stays further from the active site, located on the way to bulk solvent.

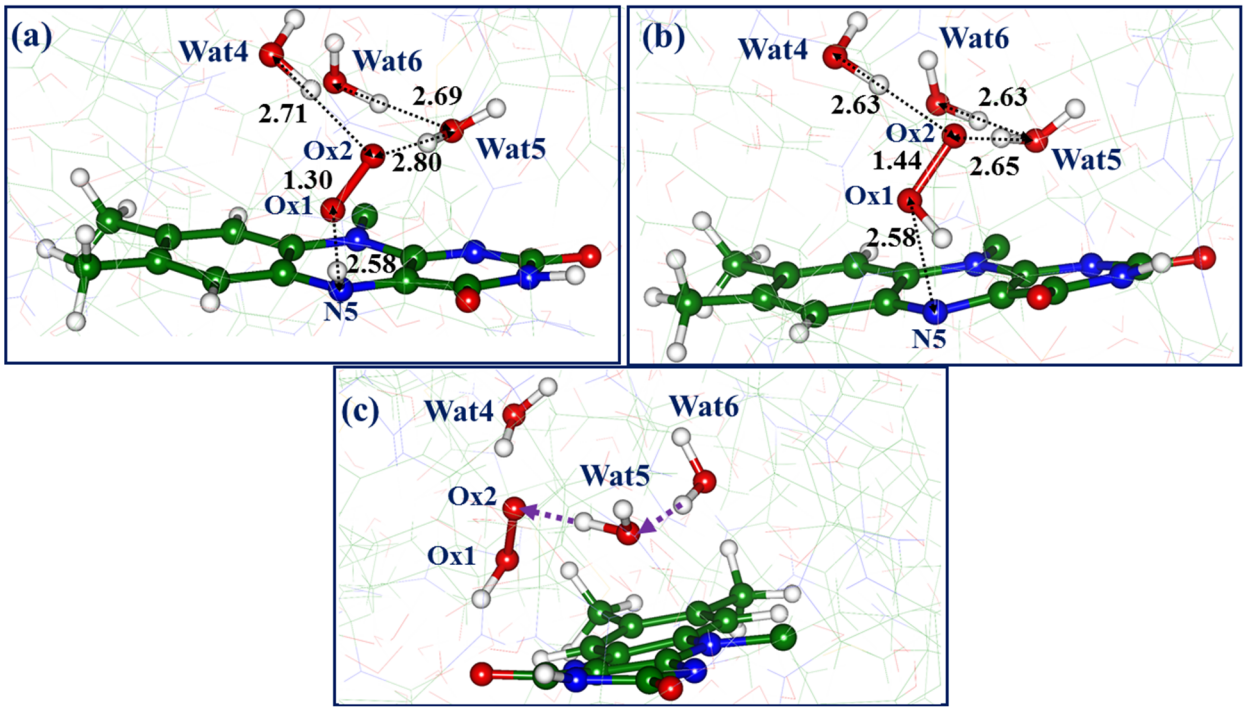

Figure 4. Pathway-2: (**a**) Triplet state complex Fl_{red}-O_2 (Complex-2) formed at the *si*-side. (**b**) Singlet state system with the hydroperoxide anion. (**c**) A possible route to the reaction products, Fl_{ox} ... H_2O_2 ... OH^-(Wat6). Magenta arrows show a proton transfer path from Wat6.

Analysis of the electronic structure in Complex-2 in the triplet and singlet states using CASSCF(14/10) calculations was carried out similarly to that described in the preceding subsection for Complex-1. Like the previous case, the dominant electronic configuration corresponds to the superoxide structure, and the energy gap between the triplet and singlet states in Complex-2 is small (about 1.6 kcal/mol).

The system shown in Figure 4b corresponds to the minimum energy structure at the singlet state PES obtained in unconstrained QM/MM minimization initiated from the structure of Complex-2. The hydroperoxide anion HO_2^- (hydrogen-bonded to water molecules Wat4, Wat5) is obtained as a result of a barrier-less transfer of the hydrogen atom transfer from N5. The QM/MM energy of the model system shown in Figure 4b is 7.8 lower than the energy of Complex-2.

Subsequent molecular events may develop along different scenarios. First, if a substrate is present in the protein cavity, the hydroperoxide anion may serve as an oxidative agent. Second, a proton from the neighboring water molecules (here, Wat5 or Wat4) may be transferred to the HO_2^- species, leading to the hydrogen peroxide molecule (see Figure 4c for the scenario with Wat5 as a proton donor). The obtained hydroxyl anion (here, in the vicinity of the isoalloxazine ring) may serve as the oxidative agent if a substrate is located nearby. Third, a more extended chain of proton transfer events may take place over proton wires, borrowing a proton from bulk, which finally removes the charged species away from the oxidized FMN. Such proton wires involving a number of water molecules are present in this system (see Figure 1). Proton transfer events over the aligned chains of water molecules are characterized by low energy barriers within 10 kcal/mol [25]; thus, these pathways are feasible.

The $S_0 \rightarrow S_1$ and $S_0 \rightarrow S_2$ excitation energies computed at the XMCQDPT2 level at the configuration shown in Figure 4b are 2.46 eV (503 nm, 0.20 o.s.) and 3.60 eV (344 nm, 0.13 o.s.). The absorption band maxima are close to those expected for the oxidized flavin in the protein environment. We conclude that pathway-2 describes the mechanism of flavin oxidation $Fl_{red}^- + O_2$ (+H_2O) $\rightarrow$ Fl_{ox} + H_2O_2 +OH^- in RutA in the absence of the substrate via the occurrence of the transient hydroperoxyl species.

2.3. Pathway-3: Oxygen-N5 Interaction from the Re-Side Oxygen Pocket

The scenario described in the preceding subsection (pathway-2) is also an option when starting from one more triplet-state flavin-oxygen complex, but this time, the oxygen molecule is located at the *re*-side pocket. The occurrence of the oxygen molecule at the *re*-side is detected in the X-ray structure PDB ID 6SGG [6]. According to the results of the crystallography analysis, the distance between the N5 atom of flavin and the nearest oxygen atom of O_2 is unusually short—2.1 Å, whereas the other oxygen atom is coordinated by the nitrogen atom of the Asn134 side chain (the distance is 2.6 Å) and the oxygen atom of the Thr105 side chain (the distance is 2.7 Å) [6]. The oxygen-binding pocket at the *re*-side was also characterized in our previous simulations [11,12], although no such short nitrogen-oxygen distance as 2.1 Å was observed in these simulations. Another important result of [12] is that the switch from the triplet state PES to the singlet state PES at some MD trajectory frame of the flavin-oxygen complex led to the barrier-less formation of the hydroperoxide anion HO_2^-, similar to what we describe in the preceding subsection of this paper.

The structure of the triplet state flavin-oxygen complex with O_2 from the *re*-side as obtained in QM/MM optimization in the present work (Complex-3) is shown in Figure 5a. We note that the dioxygen moiety again should be assigned to a superoxide O_2^-; the Ox1-Ox2 distance is 1.31 Å and the charge of the dioxygen is close to -1. The geometry configuration differs from the structure PDB ID 6SGG [6]—the dioxygen is hydrogen-bonded to flavin, Thr105, and water, whereas the Ox1-N(Asn134) distance is considerably longer (3.3 Å vs. 2.6 Å in the crystal), as well as the Ox1-N5 distance (2.6 Å vs. 2.1 Å in the crystal).

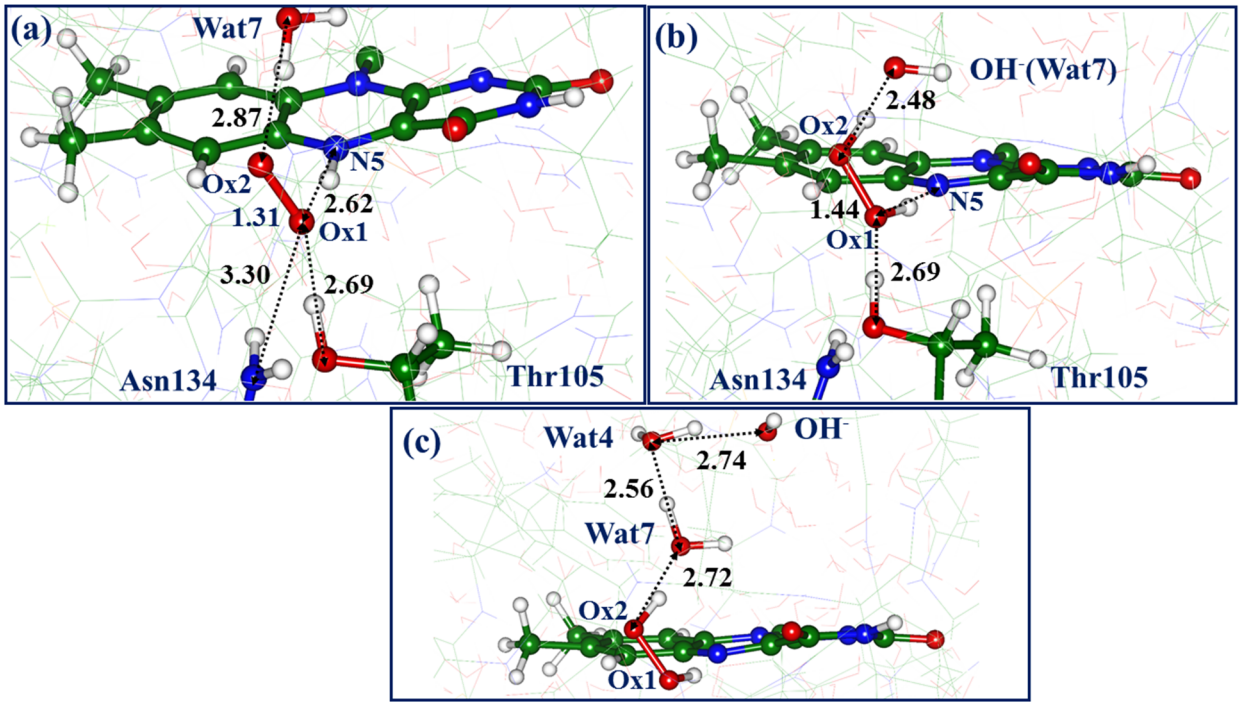

Figure 5. Minimum energy points on potential energy surfaces along pathway-3. (**a**) Triplet state complex. (**b**) Oxidized flavin and hydrogen peroxide with the nearby hydroxyl species. (**c**) Oxidized flavin, hydrogen peroxide, and the remote hydroxyl species.

The results of the CASSCF(14/10) analysis of the electronic structure of Complex-3 (see Figure 6) show that the dominant electronic configuration in the triplet state multi-configurational function corresponds to the superoxide structure of dioxygen, whereas the singlet state configuration features an even higher electron population in the dioxygen orbitals. The energy gap between the triplet and singlet states in Complex-3 computed

at the CASSCF level is small (1.1 kcal/mol), similar to all flavin-oxygen complexes in the active site of RutA.

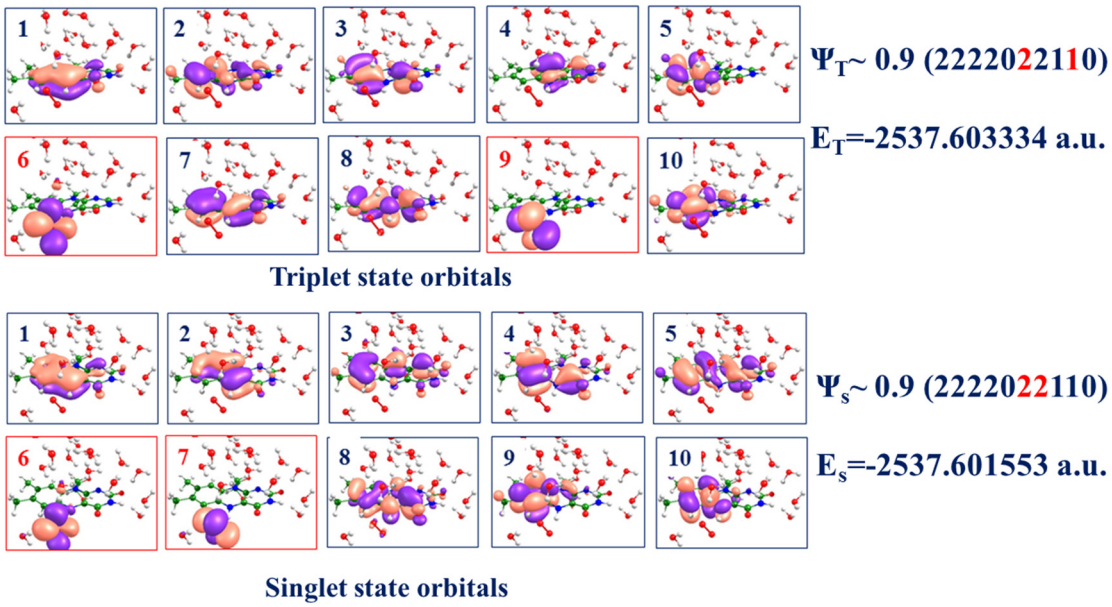

Figure 6. Results of the CASSCF(14/10)/cc-pVDZ calculations for Complex-3 (Figure 5a). The legends on the right side show a dominant electronic configuration and its weight in the triplet state and singlet state CASSCF wavefunctions composed of the active orbitals illustrated in ten boxes. The occupancies of the sixth and ninth orbitals in the triplet state or the sixth and seventh orbitals in the singlet state, mainly assigned to dioxygen, are distinguished by the red color.

At least two minimum energy structures can be located on the singlet state PES using the QM/MM calculations. The structure shown in Figure 5b is almost isoenergetic with the triplet state Complex-3. Consistent with pathway-2 (see Figure 4b), the dioxygen borrows a hydrogen atom from N5 to Ox1. In pathway-3, the increased electron population on dioxygen leads to the spontaneous formation of hydrogen peroxide at the expense of a nearby water molecule, Wat7. The structure shown in Figure 5c is 6.8 kcal/mol lower in energy than the initial Complex-3. The chain of water molecules provides a suitable proton wire to move the negative charge of the hydroxyl farther away from the isoalloxazine ring.

The $S_0 \rightarrow S_1$ and $S_0 \rightarrow S_2$ excitation energies computed at the XMCQDPT2 level for the system shown in Figure 5b are 2.46 eV (503 nm, 0.20 o.s.) and 3.64 eV (344 nm, 0.20 o.s.). They are almost the same as the reaction products at pathway-2 (see Figure 4b) and close to those of the oxidized flavin in the protein environment. We conclude that pathway-3 (as well as pathway-2) describes the mechanism of flavin oxidation $Fl_{red}^{-} + O_2 (+H_2O) \rightarrow Fl_{ox} + H_2O_2 + OH^{-}$ in RutA in the absence of a substrate.

2.4. Pathway-4: Formation of the N(5)-oxide Adducts

An intriguing pathway-4 also starts from the triplet state flavin-oxygen complex (Complex-4) at the *re*-side, although it should be noted that its QM/MM energy is 5.6 kcal/mol higher than the energy of Complex-3. The structure shown in Figure 7a differs from the previously described Complex-3 by the arrangement of the dioxygen—the Ox1-N5 distances are the same (2.62 Å) in both cases, but the Ox2 atom points towards Wat7 in Complex-3 and towards Asn134 in Complex-4. The latter structure shows poor coordination of dioxygen by the Thr105 side chain—the distance of 3.80 Å between Ox1 and the hydroxyl oxygen of Thr105 is long enough. Like all previously described flavin-oxygen complexes, Complex-4 accommodates the superoxide anion in the protein cavity—the Ox1-Ox2-distance is 1.32 Å; the charge of dioxygen is close to -1; and the energy gap between the triplet and singlet states is small.

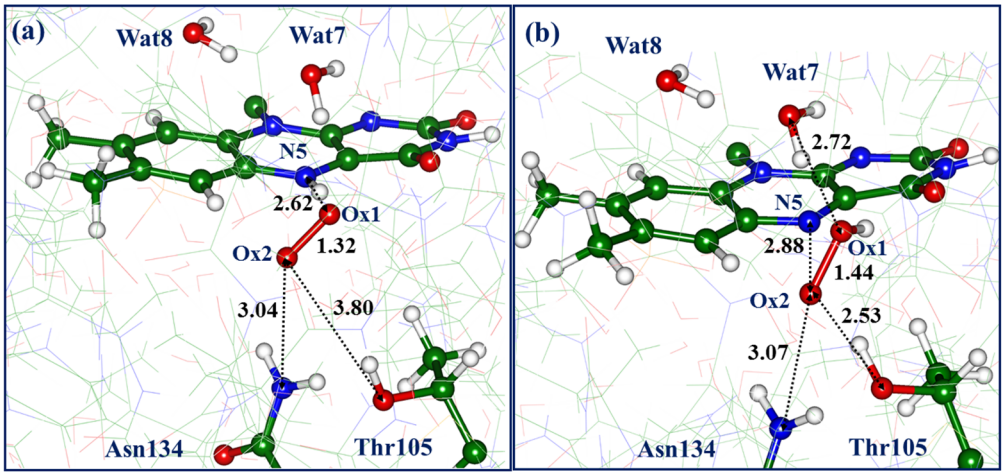

Figure 7. Pathway-4: (**a**) The initial triplet state, Complex-4. (**b**) Singlet state minimum energy point with the hydroperoxyl.

Switching to the singlet-state PES at this point and subsequent unconstrained geometry optimization led to the structure (Figure 7b) with the hydroperoxyl and Ox1-Ox2 distance of 1.44 Å. The energy of this structure is 12.8 kcal/mol lower than the level of the initial Complex-4. It is important to note the following distances: Ox2-N5 (2.88 Å) and Ox1-O(Wat7) (2.72 Å). We note in passing that all QM/MM optimized structures in both triplet and singlet states of model systems do not reveal a short oxygen-nitrogen distance of 2.09 Å between any of the dioxygen atoms and the N5 flavin atom reported in the crystal structure PDB ID 6SGG [6]; no values less than 2.5 Å were obtained in simulations.

A gradual decrease of the Ox2-N5 distance results in the formation of the N-O covalent bond with a simultaneous break of the Ox1-Ox2 bond and finally leads to the formation of the flavin-N(5)-oxide, as shown in Figure 8a. This N5-O adduct is responsible for flavin functionalization in the flavoenzyme EncM [5,6]. According to the present QM/MM calculations, its energy is 28.5 kcal/mol lower than the energy of Complex-4. This agrees with the results of quantum chemistry gas-phase calculations of the reaction of the reduced lumiflavin with the oxygen molecule leading to the lumiflavin-N(5)-oxide described in [5]—the computed reaction energy is about −23 kcal/mol. Moreover, the reaction scheme depicted in Figure 4 in [5] seems consistent with the mechanism revealed in the present QM/MM simulations of the protein. As shown in Figure 7b, the hydroxyl Ox1-H^- formed after the cleavage of the Ox1-Ox2 bond interacts with the water molecule Wat7, leading to a newly formed water molecule Wat9 and a hydroxyl anion.

The $S_0 \rightarrow S_1$ and $S_0 \rightarrow S_2$ excitation energies computed at the XMCQDPT2 level at the configuration shown in Figure 8a are 2.44 eV (508 nm, 0.12 o.s.) and 3.25 eV (381 nm, 0.16 o.s.). These values may be compared to the absorption band maxima of 463 nm (2.69 eV) and 360–380 nm (3.26–3.44 eV) of the flavin-N(5)-oxide reported for the EncM protein (see Figure S5 in [5]). Taking into account possible errors in calculations of excitation energies in complex systems [26], the agreement is reasonable; moreover, the presence of the charged species OH^- near the chromophore in our model system (Figure 8a) may cause some shifts in the computed excitation energies.

As shown in Figure 8a,b, the N(5)-oxide undergoes a further transformation, namely, the hydroxyl emerged from Wat7 (Figure 7b) attaches a proton from Wat8, stimulating the newly derived hydroxyl (from Wat8) to attack flavin at the C8 position to form a new covalent bond. This adduct refers to the C(8)-hydrated N(5)-oxide compound shown in Figure 8b. These two structures are almost degenerate in energy. The hydration reaction of a chromophore in photoactive proteins upon light illumination is known, e.g., in the Dreiklang protein [27–29]; here, this reaction may occur at the ground singlet state PES.

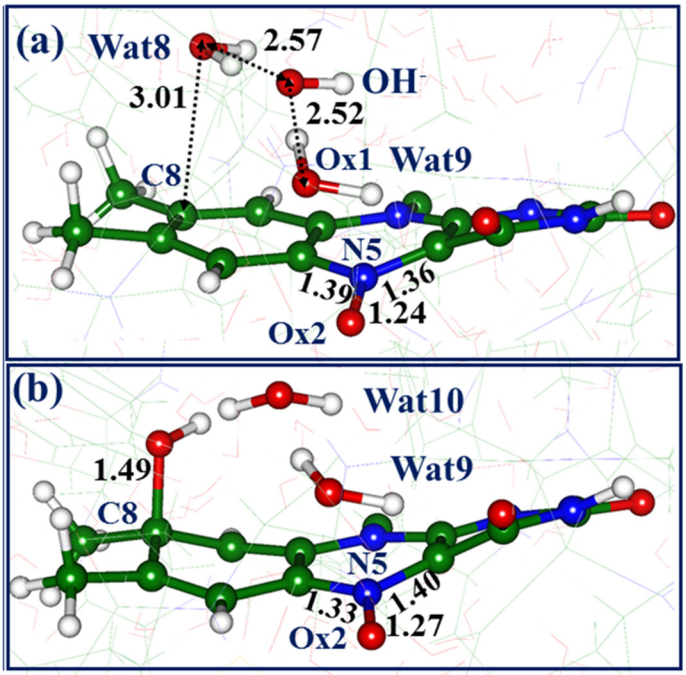

Figure 8. Singlet state minimum energy structures along Pathway-4. (**a**) The N(5)-oxide flavin-oxygen adduct. (**b**) The C(8)-hydrated N(5)-oxide flavin-oxygen adduct.

The $S_0 \rightarrow S_1$ and $S_0 \rightarrow S_2$ excitation energies computed at the XMCQDPT2 level for the system shown in Figure 8b are 2.73 eV (454 nm, 0.38 o.s.) and 3.54 eV (350 nm, 0.12 o.s.). We see a considerable change in the $S_0 \rightarrow S_1$ band (from 508 nm to 454 nm) due to chromophore hydration. This shift is clear as the electronic structure of flavin is closer to the Fl_{ox} for the flavin-N(5)-oxide and closer to the Fl_{red} for the flavin- C(8)-hydrated N(5)-oxide. The chemical formulas of both species are given in Scheme 2. We note a change in the conjugation patterns consistent with the equilibrium geometry structures (see, e.g., the distances between N5 and carbon atoms in Figure 8).

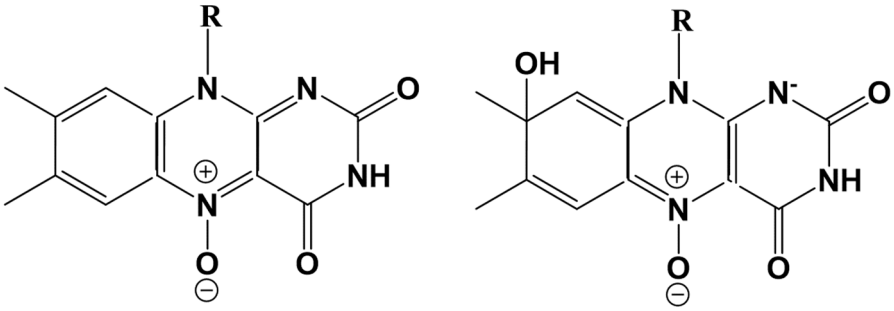

Scheme 2. Left—flavin-N(5)-oxide; right—flavin-C(8)-hydrated N(5)-oxide.

2.5. Pathway-5: Formation of the C(6)-hydroperoxyflavin Species from the Si-Side Oxygen Pocket

Finally, we describe an uncommon pathway in flavin functionalization that explores the C6 position of the isoalloxazine ring. Spontaneous covalent binding of the hydroperoxide at the C6 atom was noted in the molecular dynamics simulations with the QM/MM potentials for the RutA-O2-uracil model system [12]. The occurrence of the reaction intermediates with the C6-O bond formation was discussed in the recent study [30].

Figure 9a shows a fragment of the triplet-state model system (Complex-5) formed from the *si*-side oxygen pocket. The energy of this structure is 5.4 kcal/mol higher than that of Complex-1, which initiates the formation of the flavin-C(4a) adduct, and is 6.9 kcal/mol higher as compared to Complex-2, which gives rise to the oxidized flavin and hydrogen peroxide.

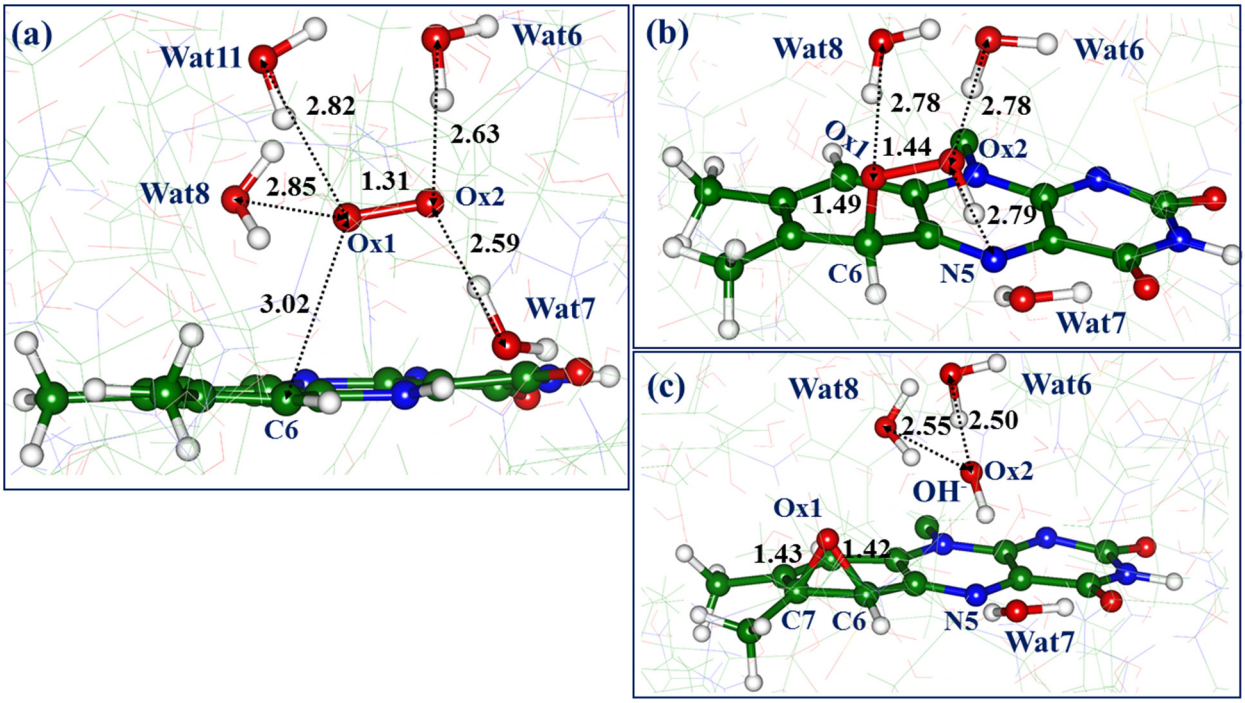

Figure 9. Structures along pathway-5: (**a**) Triplet state minimum energy point with the dioxygen moiety (Complex-5). (**b**) Structure with the flavin-C(6)-hydroperoxide adduct. (**c**) Structure with the C(6)-C(7)-epoxide adduct.

Complex-5 shows the features common to all flavin-oxygen complexes considered in the present work: the Ox1-Ox2 distance is 1.31 Å; the charge on dioxygen is close to -1; the triplet-singlet gap is small; and the dioxygen moiety is hydrogen bonded to the nearest molecular groups, in this case, to four water molecules: Wat6, Wat7, Wat8, and Wat11. The shortest distance to the atoms of the isoalloxazine ring refers to the Ox1-C6 separation—3.02 Å.

Starting from Complex-5, a structure shown in Figure 9b with the flavin-C(6)-hydroperoxide adduct (noted in the previous QM/MM MD simulations [12]) is readily obtained after switching from the triplet state PES to the singlet state PES as a result of the forming covalent bond C6-Ox1 coupled with proton transfer from N5 to Ox2. The energy of this structure is 6.5 kcal/mol lower than that of Complex-5. Principally, this pathway may proceed further; a potential barrier of about 14 kcal/mol is required to break the Ox1-Ox2 bond and to arrive at the structure shown in Figure 9c with the C(6)-C(7)-epoxide. Such cyclic patterns were noted earlier in the modeling reactions of oxygen with the chromophore of the green fluorescent protein [22]. The energy of the thus obtained structure (Figure 9c) is 30.1 kcal/mol lower than that of Complex-5, and this adduct may occur as a possible reaction intermediate. Its $S_0 \rightarrow S_1$ excitation energies computed at the XMCQDPT2 level is 2.57 eV (483 nm, 0.06 o.s.).

2.6. Summary and Concluding Remarks

In this work, we apply QM/MM and quantum chemistry methods to characterize minimum energy points on the triplet state and singlet state potential energy surfaces along the possible reaction pathways initiated by the interaction of the oxygen molecule with the molecular groups in the protein cavities of the flavoenzyme RutA. Table 1 summarizes the most important results of these simulations, grouped as the oxygen activation pathways, starting from the oxygen-containing pockets at the *si*-side and *re*-side of the flavin's isoalloxazine ring.

Table 1. Summary of the computed data along the revealed reaction pathways.

Pathway	Energies of the Initial Complexes, kcal/mol	Reaction Products	Energies of Products, kcal/mol	Absorption Band Maxima, nm (Oscillator Strengths)
		***Si*-side complexes**		
1	+1.5	C(4a)-peroxide	−16.8	357 (0.57)
2	0	$Fl_{ox} + H_2O_2 + OH^-$	−7.8	503 (0.20), 344 (0.13)
5	+6.9	Flavin-C(6)-hydroperoxide	−6.5	483 (0.06)
		Flavin-C(6)-C(7)-epoxide	−31.0	
		***Re*-side complexes**		
3	0	$Fl_{ox} + H_2O_2 + OH^-$	−6.8	503 (0.20), 341 (0.20)
4	+5.6	Flox + HO_2^-	−12.8	508 (0.12), 381 (0.16)
		Flavin-N(5)-oxide	−28.5	454 (0.38), 350 (0.12)
		Flavin-C(8)-hydrated N(5)-oxide	−28.4	

In Table 1, we compare the energies of the initial triplet state flavin-oxygen complexes (column 2) and of the corresponding reaction products (column 4) differently for the structures emerging from either the *si*-side or *re*-side oxygen pockets, despite the fact that these model systems were created for the same QM-MM partitioning scheme described below in Section 3. As clarified in Figure 1, the *re*-side region is deeper in the protein macromolecule, whereas the *si*-side is entirely in the solvent-accessible cavity. It is practically impossible to provide fully equivalent conditions for the QM/MM geometry optimization in these two regions because of the different impacts of the large amount of water molecules in the MM subsystem. For instance, the total QM/MM energies for the *re*-side initial flavin-oxygen systems (Complexes-3 and 4) are about 15 kcal/mol lower than the energies of the *re*-side initial complexes.

Analysis of the data collected in Table 1 allows us to conclude that pathways 1, 2, and 3 may refer to the most probable reaction routes leading to oxygen activation in RutA if the estimated energy barriers are considered. Pathways 2 and 3 are practically similar despite the different starting positions of the oxygen molecule—from the protein interior or from the solvent-accessible cavity. These routes describe the formation of the oxidized flavin, hydrogen peroxide, and the hydroxyl anion with a reaction energy of 7–8 kcal/mol. The computed absorption band maxima (the last column in Table 1) are the same in the two pathways showing characteristic features of the oxidized flavin. Pathway-1 leading to the formation of the flavin-C(4a)-peroxide well-known from experimental studies is also highly likely, as validated by the computed relative energies and absorption spectra.

Pathways 4 and 5 are initiated from the structures, which may be less populated considering the computed energies (6–7 kcal/mol above the level of the lowest-energy structures on the respective side) of Complex-4 and Complex-5. However, the products of the corresponding reactions, whose energies are low enough relative to the level reactants, are very interesting and describe the known [3–7] and newly characterized covalent flavin-oxygen adducts.

The computed energies of the reaction products (column 4 in Table 1) are large enough to expect that the corresponding species may be detected experimentally. The computed excitation energies and oscillator strengths are reported for every reaction product, providing useful data to analyze transient absorption bands in prospective spectral studies.

Next, we emphasize the essential role of water molecules and of proton transfer along hydrogen bond networks involving water molecules in the solvent-accessible protein cavities of RutA. This refers to all pathways studied here, and it is important to note that proton transfer over the aligned chains of water molecules is characterized by low energy barriers—within 10 kcal/mol, e.g., according to [25].

Finally, we comment that the energy profiles connecting these minimum energy points are roughly estimated in the present QM/MM calculations. We point out that there are unavoidable errors in the estimates of the activation barriers on reaction routes calculated by the QM/MM method with the modern quantum chemistry software packages, amounting to several kcal/mol [31].

3. Models and Methods

Model molecular systems were created as follows: The coordinates of heavy atoms were taken from the crystal structure PDB ID 6SGG [6] containing the oxidized FMN. We added hydrogen atoms using molecular mechanics tools, assuming that the side chains of Arg and Lys were positively charged and that the side chains of Glu and Asp were negatively charged. The reduced form of FMN was constructed. The oxygen molecules were added to the protein cavities near the isoalloxazine ring. The visual molecular dynamics (VMD) program [32] was applied to build the solvation water shells shown in Figure 1. Classical molecular dynamics simulations were carried out with the NAMD program [33] using the CHARMM36 force field [34] to equilibrate the system composed of more than 42,000 atoms. The charge of the reduced FMN species was -3, whereas the charge of the entire model system was -4.

In QM/MM optimization, a large fraction of the active site was assigned to the QM-part (Figure 10). Specifically, all atoms of FMN with the phosphate group, the oxygen molecule, the side chains of Thr105, Asn134, Trp139, Glu292, and 19 water molecules were included in the QM subsystem, which comprises 150 atoms. The Thr105 and Asn134 side chains contribute to the coordination of the dioxygen at the *re*-side; the Trp139 and Glu292 side chains border the solvent-accessible protein cavity at the *si*-side. Four hydrogen link atoms were added to the carbon atoms highlighted in yellow in Figure 10 to saturate the broken covalent bonds C_α-C_β for Thr105, Asn134, Trp139, or the C_β-C_γ bond for Glu292.

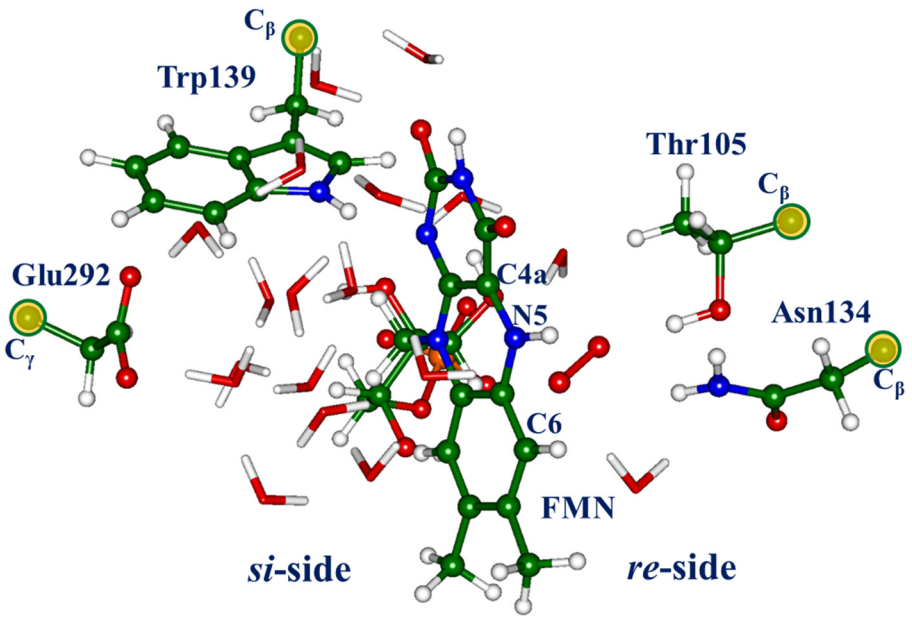

Figure 10. The QM subsystem for QM/MM calculations. Water molecules are shown as sticks. The carbon atoms at the broken covalent bonds (C_β for Thr105, Asn134, Trp139, and C_γ for Glu292) are highlighted in yellow.

Optimization of the geometry parameters and calculation of energies were performed with the NWChem software package [35]. The density functional theory PBE0 functional [36] with the D3 correction [37] and the 6–31G* basis set were used in the QM part, whereas the AMBER99 force field parameters [38] were applied to describe the MM subsystem. The electrostatic embedding scheme was used to polarize the QM region by the

Coulomb potential due to MM charges (see the relevant discussion in [31]). The unrestricted DFT approach was used in QM/MM calculations of energies and forces for the triplet state model systems, and the restricted DFT approximation was applied for the singlet state systems. No constraints were imposed in the geometry optimization of minimum energy stationary points. Crude estimates of the energy profiles near possible barriers were carried out using constrained minimization.

The state-averaged CASSCF method with the distribution of 14 electrons over 10 complete active orbitals represented by the cc-pVDZ basis set was used to analyze the electronic structure of the flavin-oxygen complexes for a large molecular cluster identical to the QM subsystem in QM/MM simulations. To select the CASSCF scheme, we carried out a series of preliminary calculations at the configuration interaction level to recognize the orbitals that must be assigned to the active space. Further enlargement of the active space is not technically feasible.

The optimized active orbitals for Complex-1 and Complex-3 are illustrated in Figures 3 and 6. Calculations of the vertical excitation energies and oscillator strengths were carried out using the extended multiconfigurational quasi-degenerate perturbation theory in the second order (XMCQDPT2) [16] based on the SA-CASSCF(14/10) orbitals. All calculations for cluster models were performed using the Firefly package [39].

4. Conclusions

We show that various location sites of the oxygen molecule in the solvent-accessible protein cavities initiate various reaction pathways of flavin functionalization in the flavoenzyme RutA in the absence of the substrate. Several triplet state complexes of the molecular oxygen with the reduced flavin mononucleotide are optimized at both the *re*-side and *si*-side of the isoalloxazine ring of flavin using the QM/MM method. In every complex, the dioxygen moiety in the protein cavity is best described as the superoxide anion O_2^- interacting with the flavin semiquinone. Reactions on the singlet state potential energy surface can follow several pathways. Along these pathways, the formation of the following products occurs: oxidized flavin and hydrogen peroxide, or covalent flavin-oxygen adducts such as C(4a)-peroxide, N(5)-oxide, or C(6)-hydroperoxide. Novel variants of the adducts—C(8)-hydrated N(5)-oxide and C(6)-hydroperoxide—are characterized as the minimum energy structures in the model protein-oxygen system. Excitation energies and oscillator strengths are estimated for the reaction products. The results of the present simulations contribute to the studies of molecular processes of flavin functionalization and the factors that govern oxygen reactivity in flavoenzymes, taking RutA as an important example.

Supplementary Materials: The following supporting information can be downloaded at https://www.mdpi.com/article/10.3390/molecules28052405/s1. Section S1: Description of the files with the atomic coordinates (pdb-format) of the structures optimized in QM/MM calculations that are deposited to the general-purpose open-access repository ZENODO (can be accessed via https://doi.org/10.5281/zenodo.7558382). Section S2: A sample input file for the QM/MM optimization using the NWChem program. Section S3: A sample input file for CASSCF and XMCQDPT2 calculations using the Firefly program.

Author Contributions: Conceptualization, B.G., T.D. and A.N.; methodology, B.G., T.D. and A.N.; validation, B.G., T.D. and A.N.; formal analysis, B.G., T.D. and A.N.; investigation, B.G., T.D. and A.N.; data curation, B.G., T.D. and A.N.; writing—original draft preparation, A.N; writing—review and editing, B.G., T.D. and A.N.; visualization, B.G. and A.N.; supervision, A.N.; project administration, A.N.; funding acquisition, B.G. All authors have read and agreed to the published version of the manuscript.

Funding: This research was funded by the Russian Science Foundation, grant number 22-13-00012.

Data Availability Statement: The files with atomic coordinates of the stationary points on potential energy surfaces in the pdb-format are deposited to the general-purpose open-access repository ZENODO, which can be accessed via https://doi.org/10.5281/zenodo.7558382 (accessed on 26 January 2023).

Acknowledgments: The research was carried out using equipment in the shared research facilities for high-performance computing resources at Lomonosov Moscow State University. The use of supercomputer resources at the Joint Supercomputer Center of the Russian Academy of Sciences is acknowledged.

Conflicts of Interest: The authors declare no conflict of interest.

References

1. Palfey, B.A.; McDonald, C.A. Control of catalysis in flavin-dependent monooxygenases. *Arch. Biochem. Biophys.* **2010**, *493*, 26–36. [CrossRef] [PubMed]
2. Loh, K.D.; Gyaneshwar, P.; Papadimitriou, E.M.; Fong, R.; Kim, K.S.; Parales, R.; Zhou, Z.; Inwood, W.; Kustu, S. A previously undescribed pathway for pyrimidine catabolism. *Proc. Natl. Acad. Sci. USA* **2006**, *103*, 5114–5119. [CrossRef] [PubMed]
3. Romero, E.; Gómez Castellanos, J.R.; Gadda, G.; Fraaije, M.W.; Mattevi, A. Same substrate, many reactions: Oxygen activation in flavoenzymes. *Chem. Rev.* **2018**, *118*, 1742–1769. [CrossRef] [PubMed]
4. Adak, S.; Begley, T.P. RutA-catalyzed oxidative cleavage of the uracil amide involves formation of a flavin-N5-oxide. *Biochemistry* **2017**, *56*, 3708–3709. [CrossRef]
5. Saleem-Batcha, R.; Stull, F.; Sanders, J.N.; Moore, B.S.; Palfey, B.A.; Houk, K.N.; Teufel, R. Enzymatic control of dioxygen binding and functionalization of the flavin cofactor. *Proc. Natl. Acad. Sci. USA* **2018**, *115*, 4909–4914. [CrossRef]
6. Matthews, A.; Saleem-Batcha, R.; Sanders, J.N.; Stull, F.; Houk, K.N.; Teufel, R. Aminoperoxide adducts expand the catalytic repertoire of flavin monooxygenases. *Nat. Chem. Biol.* **2020**, *16*, 556–563. [CrossRef]
7. Toplak, M.; Matthews, A.; Teufel, R. The devil is in the details: The chemical basis and mechanistic versatility of flavoprotein monooxygenases. *Arch. Biochem. Biophys.* **2021**, *698*, 108732. [CrossRef] [PubMed]
8. Teufel, R.; Miyanaga, A.; Michaudel, Q.; Stull, F.; Louie, G.; Noel, J.P.; Baran, P.S.; Palfey, B.; Moore, B.S. Flavin-mediated dual oxidation controls an enzymatic Favorskii-type rearrangement. *Nature* **2013**, *503*, 552–556. [CrossRef]
9. Kar, R.K.; Miller, A.F.; Mroginski, M.A. Understanding flavin electronic structure and spectra. *WIREs Comput. Mol. Sci.* **2022**, *12*, 1541. [CrossRef]
10. Luo, Y.; Liu, Y.J. Theoretical Insight into a Nonadiabatic Proton-Coupled Electron Transfer Mechanism of Reduced Flavin Oxygenation. *J. Phys. Chem. A* **2019**, *123*, 4354–4359. [CrossRef]
11. Polyakov, I.V.; Domratcheva, T.M.; Kulakova, A.M.; Nemukhin, A.V.; Grigorenko, B.L. Computational Modeling of the Interaction of Molecular Oxygen with the Flavin-Dependent Enzyme RutA. *Supercomp. Front. Innov.* **2022**, *9*, 46–55. [CrossRef]
12. Polyakov, I.V.; Nemukhin, A.V.; Domratcheva, T.M.; Kulakova, A.M.; Grigorenko, B.L. Quantum-based modeling of protein-ligand interaction: The complex of RutA with uracil and molecular oxygen. *Mol. Inform.* **2022**, *41*, 2200175. [CrossRef] [PubMed]
13. Kabir, M.P.; Orozco-Gonzalez, Y.; Gozem, S. Electronic spectra of flavin in different redox and protonation states: A computational perspective on the effect of the electrostatic environment. *Phys. Chem. Chem. Phys.* **2019**, *21*, 16526–16537. [CrossRef]
14. Kar, R.K.; Borin, V.A.; Ding, Y.; Matysik, J.; Schapiro, I. Spectroscopic properties of Lumiflavin: A quantum chemical study. *Photochem. Photobiol.* **2019**, *95*, 662–674. [CrossRef]
15. Schwinn, K.; Ferré, N.; Huix-Rotllant, M. UV-visible absorption spectrum of FAD and its reduced forms embedded in a cryptochrome protein. *Phys. Chem. Chem. Phys.* **2020**, *22*, 12447–12455. [CrossRef]
16. Granovsky, A.A. Extended Multi-Configuration Quasi-Degenerate Perturbation Theory: The New Approach to Multi-State Multi-Reference Perturbation Theory. *J. Chem. Phys.* **2011**, *134*, 214113. [CrossRef]
17. Gozem, S.; Huntress, M.; Schapiro, I.; Lindh, R.; Granovsky, A.A.; Angeli, C.; Olivucci, M. Dynamic Electron Correlation Effects on the Ground State Potential Energy Surface of a Retinal Chromophore Model. *J. Chem. Theory Comput.* **2012**, *8*, 4069–4080. [CrossRef]
18. Solov'yov, I.; Domratcheva, T.; Schulten, K. Separation of photo-induced radical pair in cryptochrome to a functionally critical distance. *Sci. Rep.* **2014**, *4*, 3845. [CrossRef]
19. Gozem, S.; Luk, H.L.; Schapiro, I.; Olivucci, M. Theory and Simulation of the Ultrafast Double-Bond Isomerization of Biological Chromophores. *Chem. Rev.* **2017**, *117*, 13502–13565. [CrossRef] [PubMed]
20. Nemukhin, A.V.; Grigorenko, B.L.; Khrenova, M.G.; Krylov, A.I. Computational Challenges in Modeling of Representative Bioimaging Proteins: GFP-Like Proteins, Flavoproteins, and Phytochromes. *J. Phys. Chem. B* **2019**, *29*, 6133–6149. [CrossRef]
21. Grigorenko, B.L.; Nemukhin, A.V.; Polyakov, I.V.; Morozov, D.I.; Krylov, A.I. First-Principles Characterization of the Energy Landscape and Optical Spectra of Green Fluorescent Protein along the A→I→B Proton Transfer Route. *J. Am. Chem. Soc.* **2013**, *135*, 11541–11549. [CrossRef]
22. Grigorenko, B.L.; Nemukhin, A.V.; Polyakov, I.V.; Khrenova, M.G.; Krylov, A.I. A Light-Induced Reaction with Oxygen Leads to Chromophore Decomposition and Irreversible Photobleaching in GFP-Type Proteins. *J. Phys. Chem. B* **2015**, *119*, 5444–5452. [CrossRef]
23. Polyak, I.; Reetz, M.T.; Thiel, W. QM/MM Study on the Mechanism of the Enzymatic Baeyer-Villiger Reaction. *J. Am. Chem. Soc.* **2012**, *134*, 2732–2741. [CrossRef]
24. Giuliani, G.; Melaccio, F.; Gozem, S.; Cappelli, A.; Olivucci, M. QM/MM Investigation of the Spectroscopic Properties of the Fluorophore of Bacterial Luciferase. *J. Chem. Theory Comput.* **2021**, *17*, 605–613. [CrossRef]

25. Li, C.; Voth, G.A. A quantitative paradigm for water-assisted proton transport through proteins and other confined spaces. *Proc. Natl. Acad. Sci. USA* **2021**, *118*, e2113141118. [CrossRef] [PubMed]
26. Lischka, H.; Nachtigallová, D.; Aquino, A.J.A.; Szalay, P.G.; Plasser, F.; Machado, F.B.C.; Barbatti, M. Multireference Approaches for Excited States of Molecules. *Chem. Rev.* **2018**, *118*, 7293–7361. [CrossRef]
27. Brakemann, T.; Stiel, A.C.; Weber, G.; Andresen, M.; Testa, I.; Grotjohann, T.; Leutenegger, M.; Plessmann, U.; Urlaub, H.; Eggeling, C.; et al. A Reversibly Photoswitchable GFP-Like Protein with Fluorescence Excitation Decoupled from Switching. *Nat. Biotechnol.* **2011**, *29*, 942–947. [CrossRef] [PubMed]
28. Sen, T.; Ma, Y.; Polyakov, I.V.; Grigorenko, B.L.; Nemukhin, A.V.; Krylov, A.I. Interplay between Locally Excited and Charge Transfer States Governs the Photoswitching Mechanism in the Fluorescent Protein Dreiklang. *J. Phys. Chem. B* **2021**, *125*, 757–770. [CrossRef] [PubMed]
29. Grigorenko, B.L.; Polyakov, I.V.; Nemukhin, A.V. Modeling Light-Induced Chromophore Hydration in the Reversibly Photoswitchable Fluorescent Protein Dreiklang. *Molecules* **2023**, *28*, 505. [CrossRef]
30. Iyer, A.; Reis, R.A.G.; Gannavaram, S.; Momin, M.; Spring-Connell, A.M.; Orozco-Gonzalez, Y.; Agniswamy, J.; Hamelberg, D.; Weber, I.T.; Gozem, S.; et al. A Single-Point Mutation in d-Arginine Dehydrogenase Unlocks a Transient Conformational State Resulting in Altered Cofactor Reactivity. *Biochemistry* **2021**, *6*, 711–724. [CrossRef]
31. Giudetti, G.; Polyakov, I.; Grigorenko, B.L.; Faraji, S.; Nemukhin, A.V.; Krylov, A.I. How Reproducible Are QM/MM Simulations? Lessons from Computational Studies of the Covalent Inhibition of the SARS-CoV-2 Main Protease by Carmofur. *J. Chem. Theory Comput.* **2022**, *18*, 5056–5067. [CrossRef] [PubMed]
32. Humphrey, W.; Dalke, A.; Schulten, K. VMD: Visual Molecular Dynamics. *J. Mol. Graph.* **1996**, *14*, 33–38. [CrossRef] [PubMed]
33. Phillips, J.C.; Hardy, D.J.; Maia, J.D.C.; Stone, J.E.; Ribeiro, J.V.; Bernardi, R.C.; Buch, R.; Fiorin, G.; Hénin, J.; Jiang, W.; et al. Scalable molecular dynamics on CPU and GPU architectures with NAMD. *J. Chem. Phys.* **2020**, *153*, 044130. [CrossRef] [PubMed]
34. Best, R.B.; Zhu, X.; Shim, J.; Lopes, P.E.M.; Mittal, J.; Feig, M.; MacKerell, A.D. Optimization of the Additive CHARMM All Atom Protein Force Field Targeting Improved Sampling of the Backbone ϕ, ψ and Side-Chain χ_1 and χ_2 Dihedral Angles. *J. Chem. Theory Comput.* **2012**, *8*, 3257–3273. [CrossRef] [PubMed]
35. Valiev, M.; Bylaska, E.J.; Govind, N.; Kowalski, K.; Straatsma, T.P.; Van Dam, H.J.J.; Wang, D.; Nieplocha, J.; Apra, E.; Windus, T.L.; et al. NWChem: A Comprehensive and Scalable Open-Source Solution for Large Scale Molecular Simulations. *Comput. Phys. Commun.* **2010**, *181*, 1477–1489. [CrossRef]
36. Adamo, C.; Barone, V. Toward reliable density functional methods without adjustable parameters: The PBE0 model. *J. Chem. Phys.* **1999**, *110*, 6158. [CrossRef]
37. Grimme, S.; Ehrlich, S.; Lars Goerigk, L. Effect of the damping function in dispersion corrected density functional theory. *J. Comput. Chem.* **2011**, *32*, 1456–1465. [CrossRef]
38. Ponder, J.W.; Case, D.A. Force fields for protein simulations. *Adv. Prot. Chem.* **2003**, *66*, 27–85. [CrossRef]
39. Granovsky, A.A. Firefly, Version 8. Available online: http://classic.chem.msu.su/gran/gamess (accessed on 26 January 2023).